Author/s:
Chen, C;Qin, S;Liu, D;Wang, J;Yang, G;Su, Y;Zhang, L;Cao, W;Ma, M;Qian, Y;Liu, Y;Liu, JZ;Lei, W

Title:
Ultrafast, Stable Ionic and Molecular Sieving through Functionalized Boron Nitride Membranes

Date:
2019-08-21

Citation:
Chen, C., Qin, S., Liu, D., Wang, J., Yang, G., Su, Y., Zhang, L., Cao, W., Ma, M., Qian, Y., Liu, Y., Liu, J. Z. & Lei, W. (2019). Ultrafast, Stable Ionic and Molecular Sieving through Functionalized Boron Nitride Membranes. ACS Applied Materials and Interfaces, 11 (33), pp.30430-30436. https://doi.org/10.1021/acsami.9b08296.

Ultrafast, Stable Ionic and Molecular Sieving through Functionalized Boron Nitride Membranes

Cheng Chen[‡a], Si Qin[‡a,d], Dan Liu[a], Jiemin Wang[a], Guoliang Yang[a], Yuyu Su[a], Liangzhu Zhang[a], Wei Cao[c], Ming Ma*[c], Yijun Qian[a], Yuchen Liu[a], Jefferson Zhe Liu*[b], Weiwei Lei*[a]*

[a]Institute for Frontier Materials, Deakin University, Locked Bag 2000, Geelong, Victoria 3220, Australia;

[b]Department of Mechanical Engineering, University of Melbourne, Parkville, Victoria 3010, Australia;

[c]Department of Mechanical Engineering, State Key Laboratory of Tribology, Tsinghua University, Beijing 100084, China

[d]ARC Centre of Excellence for Electromaterials Science (ACES), Australia

Corresponding Author: Email address: dan.liu@deakin.edu.au; maming16@mail.tsinghua.edu.cn; zhe.liu@unimelb.edu.au; weiwei.lei@deakin.edu.au

ABSTRACT

Porous membranes play an important role in the separation technologies such as gas purification, solutes nanofiltration and desalination. An ideal membrane should be thin to maximize permeation speed, have optimum pore sizes to maximise selectivity and be stable in various harsh conditions. Here, we show that the nanometer-thick membrane prepared by means of filtration of functionalized boron nitride (FBN) water suspensions can block solutes with hydrated radii larger than 4.3 angstroms (Å) in water. The FBN membranes with abundant nanochannels reduce the path length of ions. As molecular sieves, the FBN membrane can permeate small ions at an ultrahigh rate—a 25-fold enhancement compared with that of its theoretical diffusion rate and much higher than graphene oxide membrane. Importantly, the FBN membrane exhibits excellent permeability even when it was immersed in acidic, alkaline and basic salts solutions due to its intrinsic chemical stability. The molecular dynamics (MD) simulations further confirmed that the nanocapillaries formed within the FBN membrane in the hydrated state were responsible for the high permeation performance. The simple vacuum filtration fabricated FBN membrane with angstrom-sized channels and ultrafast permeation of ions promises great potential applications in the areas of barrier separation and water purification.

KEYWORDS: Functionalized boron nitride, membrane, molecular sieving, angstrom-sized channels, molecular dynamics (MD) simulations.

1. INTRODUCTION

During the last few decades, porous membranes with tiny and well-defined pore size, especially in the angstrom range, have exhibited plenty of intriguing advancements in filtration and separation applications[1-7]. More recently, graphene oxide (GO) and graphene membranes, have been demonstrated to be promising nanomaterials for ions and gas separations[8]. The nanoscale pores of these membranes allow gases and ions with sizes smaller than those of the pores to permeate, while block all other larger species. However, GO membranes tend to disintegrate and redisperse in water due to the surface negative charge on hydration, which is unfavourable in practical applications[9-11]. Hence, porous membranes with small pore sizes, nanometer scale thickness, high chemical and structural stability are desirable to achieve excellent selectivity and high permeability and stability in a variety of harsh conditions.

Boron nitride (BN), an analogue of graphene, consists of layered BN planes and shows a number of attractive properties compared with graphene and graphene oxide, including extremely high resistance to oxidation and outstanding chemical inertness, electrical-insulating properties, high thermal conductivity and stability[12-17]. In addition, the polarity of B-N bonds and the high surface area of BN-related nanostructures provide good adsorption properties of various substances ranging from organic pollutants[18] to hydrogen[19]. Therefore, BN nanosheets are a promising candidate as membrane material because of their intrinsic atomic thickness, mechanical robustness and relative chemical inertness[20-22]. Our group recently reported BN based membrane with ultrafast solvent transport for molecular separation driven under gas pressure and semipermeability for mixture molecules[23, 24]. However, the understanding of BN interstitial space and their effect on ions and molecules sieving are still lacking to date.

Here we report nanometer-thick functionalized boron nitride (FBN) membrane prepared by vacuum filtration of multi-layer FBN aqueous suspensions with ultrafast and controllable molecular sieving performance. The FBN membrane exhibited an unprecedented permeation of smaller ions with rates of approximate 9 mol m^{-2} h^{-1} for hydrated sodium ions, nearly 25 times faster than that of its theoretical diffusion rate. Furthermore, the membrane permeates smaller ions under acidic and basic solution without losing the efficiency of permeation due to the intrinsic strong resistance to oxidation and good chemical inertness of BN. These properties make FBN membrane a promising candidate in the applications of barrier separation and water purification.

2. EXPERIMENTAL SECTION

Theoretical calculation: To explore the free energy between BN solvated in water, we have adopted molecular dynamics (MD) simulations using LAMMPS packages[25]. Water was modelled by using the non-polarizable rigid TIP4P/2005 model. The force field of BN was taken from Tocci et al.[26], which was modelled by considering the partial charges on B and N. The cross-term interactions were estimated using the Lorentz−Berthelot mixing rules. The Lennard-Jones potential and electrostatic interactions were both truncated at a distance of 1.2 nm. Long-range electrostatic interactions were calculated with the particle−particle particle−mesh (PPPM) method. Bond lengths and angles in water molecules were constrained using the SHAKE algorithm[27]. During the simulation two BN flakes each containing five BN monolayers in the x-y plane were placed in the center of a water box with dimension of $6 \times 6 \times 8$ nm^3. The BN flakes were in the stable AA′ stacking mode and had a dimension of $2 \times 2 \times 1.34$ nm^3. Periodic boundary conditions were applied in all three dimensions.

To demonstrate the free energy between BN flakes, we calculated the potential of mean force (PMF) by numerically integrating the interaction forces required to separate the two parallel and fixed BN flakes at various intersheet separations. The free energies along the perpendicular direction was investigated and the distance d, between two BN flakes, were chosen as the reaction coordinates. The d ranges from 0.5 nm to 2.0 nm with an increment of 0.05 nm. Each simulated system was first equilibrated at 300 K and 1.0 bar for 2 ns in the NPT ensemble. The system was allowed to further relax for 1 ns in the NVT ensemble. Finally, a 4-ns production run was used for data analysis including the PMF calculations.

Preparation of FBN dispersion: Water dispersible FBN colloid was prepared by a one-step ball milling method. Commercial BN powders were first blended with urea and milled with a Pulverisette 7 (Fritsch) at room temperature for 20 h, then the mixture was dispersed in water and dialyzed for one week. The as-prepared FBN colloid could remain stable for more than 6 months at room temperature.

Membrane fabrication: FBN membranes were prepared by filtrating target amounts of FBN solution on commercial cellulose ester membrane (0.2 μm nominal pore size, Whatman). The thickness of the FBN membrane were easily adjusted by changing the amount of FBN dispersion.

Permeation test: The permeation tests were performed using a homemade device as schematically shown in Figure 1e. It contains two identical compartments with the same height separated with a membrane with an effective area of 8×10^{-2} cm^2. In a typical experiment, both compartments were first filled with water and kept for 4 h to fully hydrate the membranes. Then, the two compartments were filled with salt solution and deionised water respectively. During the test, each compartment

was capped with a rubber stopper to prevent the evaporation of the water. Both compartments were stirred using magnetic stirring to make sure the solution is homogeneous.

Monitoring ion conductivity: To monitor the ion diffusion through the FBN membrane, conductivity of the permeate solutions were recorded with a conductivity meter (WP-81 TPS). The detection limit of the conductivity meter is 0.01 μS, which correspond to a concentration of salts at μM level. The ion conductivity of the permeate solution were recorded with the conductivity meter at various time.

Quantitative analysis of ionic and molecular permeation rate: Atomic absorption spectroscopy (AAS, Varian AA140) and the inductively coupled plasma optical emission spectrometry (ICP-OES, Varian Inc.) were employed to analyse and quantify the cation and anion species in the permeation compartment, respectively. Furthermore, a total organic carbon analyser (TOC, Aurora 1030W, USA) was used to detect the organic solutes. These experiment were carried out using at least three different FBN membranes, and the results reported here were average from several measurements. The experimental ion permeation rates R can be calculated using:

$$R = I / (A \times t)$$

where I is permeated amount of the cation and anion species and organic solute molecules which are quantified by the AAS, ICP-OES and TOC measurements. A is the fixed effective membrane area (8×10^{-2} cm^2), and t is the recording time.

Ion permeation rates (J) calculation: The classical diffusion equation was used to calculate the expected diffusion rates:

$$J = D \times \Delta C \times A_{eff} / L_{eff}$$

where D is the ion diffusion coefficient in water and ΔC the concentration gradient across the membrane ($\Delta C \approx 0.2$ M). Taking FBN membrane with an area of 8×10^{-2} cm^2 for the ions sieving tests, the effective area A_{eff} of the water column through which the diffusion can occur is given by $A_{eff} \approx 8 \times 10^{-2}$ $cm^2 \times d / L \approx 8 \times 10^{-4}$ cm^2. The effective length of this column is $L_{eff} \approx L \times H / d \approx 20$ μm, where H is the thickness of the FBN membrane, d is the intersheet spacing of the FBN lamellar (22.4 - 26 Å), and L is the capillary length (lateral size of FBN nanosheets is 100-300 nm, we use 200 nm for calculation).

Characterization: XRD was performed on a Panalytical X'pert powder with Cu K radiation (λ = 0.15418 nm). Scanning electron micrographs (SEM) were taken out using a Zeiss Supra 55. Transmission electron microscope (TEM) images were performed on JEOL 2100 LaB_6 (operation at 200 kV) apparatus. Atomic force microscope (AFM) images were carried out on an Asylum Cypher. The samples for AFM tests were prepared by drop drying diluted solutions on freshly cleaved mica sheets. Fourier transform infrared (FTIR) spectroscopy was conducted with a Bruker Vertex 70 FTIR spectrometer and Raman spectra was operated with a Ranishaw Raman spectrometer with a wavelength of 633 nm. Thermogravimetric analysis (TGA) was carried out with a TA Q50 under N_2 gas condition. The contact angle was averaged with 6 data on a contact angle goniometer (CAM101, KSV).

3. RESULTS AND DISCUSSION

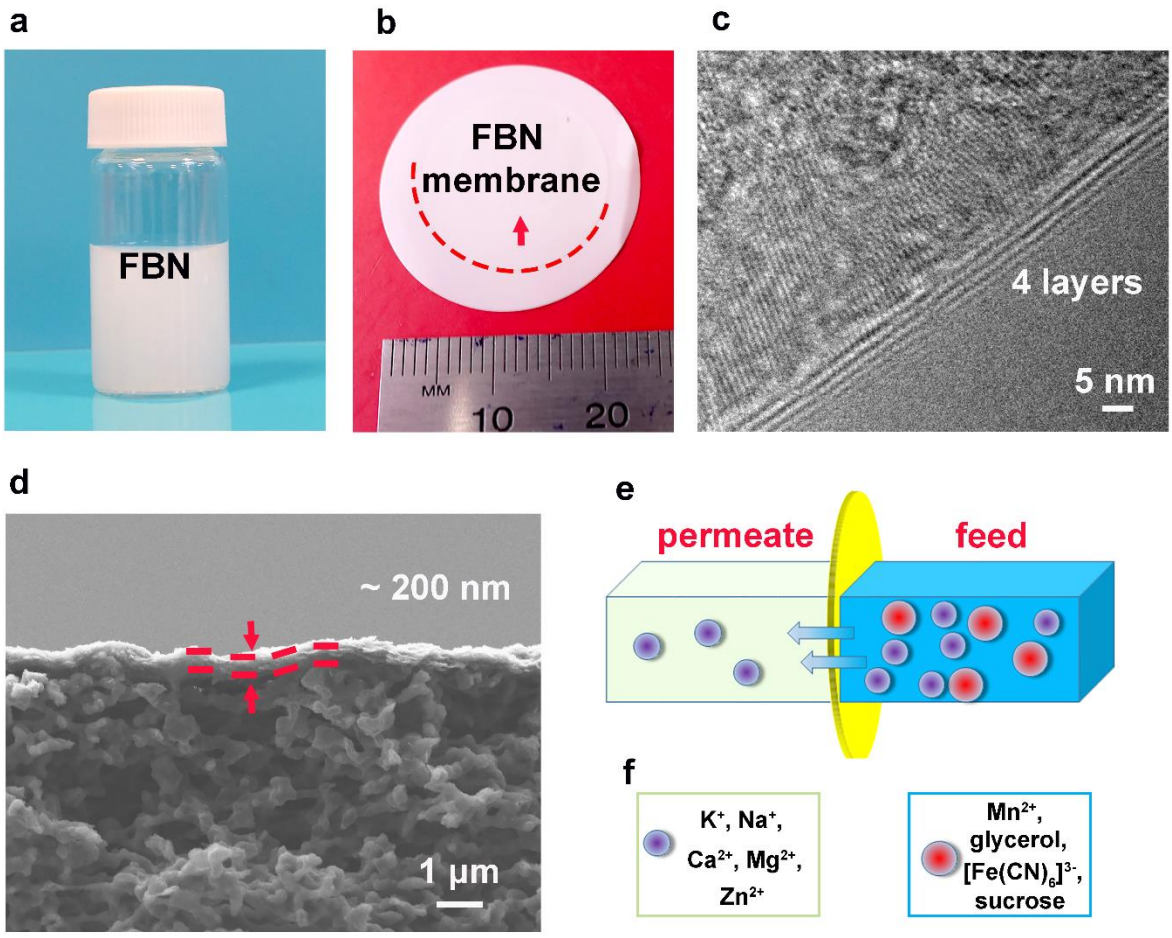

Figure 1. (a) Photograph of a FBN water dispersion. (b) Photograph of the FBN membrane. The FBN membrane was highlighted with red dash line to distinguish it from the support membrane. (c) TEM image of the edge of an FBN flake. (d) The cross-sectional SEM image of FBN membrane with a thickness of 200 nm supported on a filter membrane. (e) Schematic diagram of the permeation of different ions through FBN membranes. (f) The tested species, left box shows the ions that can pass through the FBN membrane while the right box illustrates the hydrated ions and molecules that are blocked by the FBN membrane.

FBN water suspension is prepared by a modified one-step ball-milling method using bulk BN particles with urea as the functional agent. Figure 1a shows a photograph of a 2 mg mL^{-1} FBN

suspension. FBN membranes were readily prepared by filtering the FBN water suspensions on a commercial cellulose ester membrane (Figure 1b). The cellulose ester membrane was selected as the substrate due to the flexibility and high porosity. The thickness of the FBN membrane could be changed by adjusting the volume of the FBN dispersion. Atomic force microscopy (AFM) reveals that the multilayered FBN flakes have a height of 1.2 nm with lateral dimensions of around 100-300 nm (Figure S1). Transmission electron microscopy (TEM) images further confirm that the FBN flakes constitute of 4–5 layers (Figure S1 and Figure 1c). Figure 1d shows a cross-sectional SEM image of the FBN membrane, exhibiting a laminar structure with a thickness of about 200 nm. For the results discussed in the following text, the FBN membrane was fixed at 200 nm unless stated otherwise. The XRD patterns of the prepared FBN membrane show a characteristic diffraction peak at 26.8°, which arises from the (002) plane of the FBN (Figure S2). The (002) diffraction peak is at the same position to that in bulk BN particles indicating that the interlayer spacing of the FBN remained unchanged[20].

FTIR, Raman and TGA were performed to further understand the basic structural characteristics of the FBN. The FTIR spectrum (Figure S3) shows a strong absorption centred at 1380 cm^{-1} (in-plane B–N stretching) and a vibration peak occurred at approximately 780 cm^{-1} (out-of-plane B–N–B bending vibration), respectively. Furthermore, a broad peak can be found from 3000 to 3600 cm^{-1} due to the N–H– (approximately 3250 cm^{-1}) and O–H– (approximately 3410 cm^{-1}) vibrations from the synthesis process, promoting a surface charge of the FBN flakes to be stable at high concentrations in water[23]. The Raman spectra (Figure S4) further exhibits that the FBN membranes exhibit a peak at 1367 cm^{-1} (E_{2g} vibration). TGA image (Figure S5) further suggests that ~4.3 wt% NH_2- groups are in the FBN flakes due to the presence of urea in ball-milling process[28]. FBN membrane shows a contact angle 43° verifying the produced FBN flakes

are hydrophilic (Figure S6). Therefore, the above results show that the FBN flakes are functionalized with amino groups.

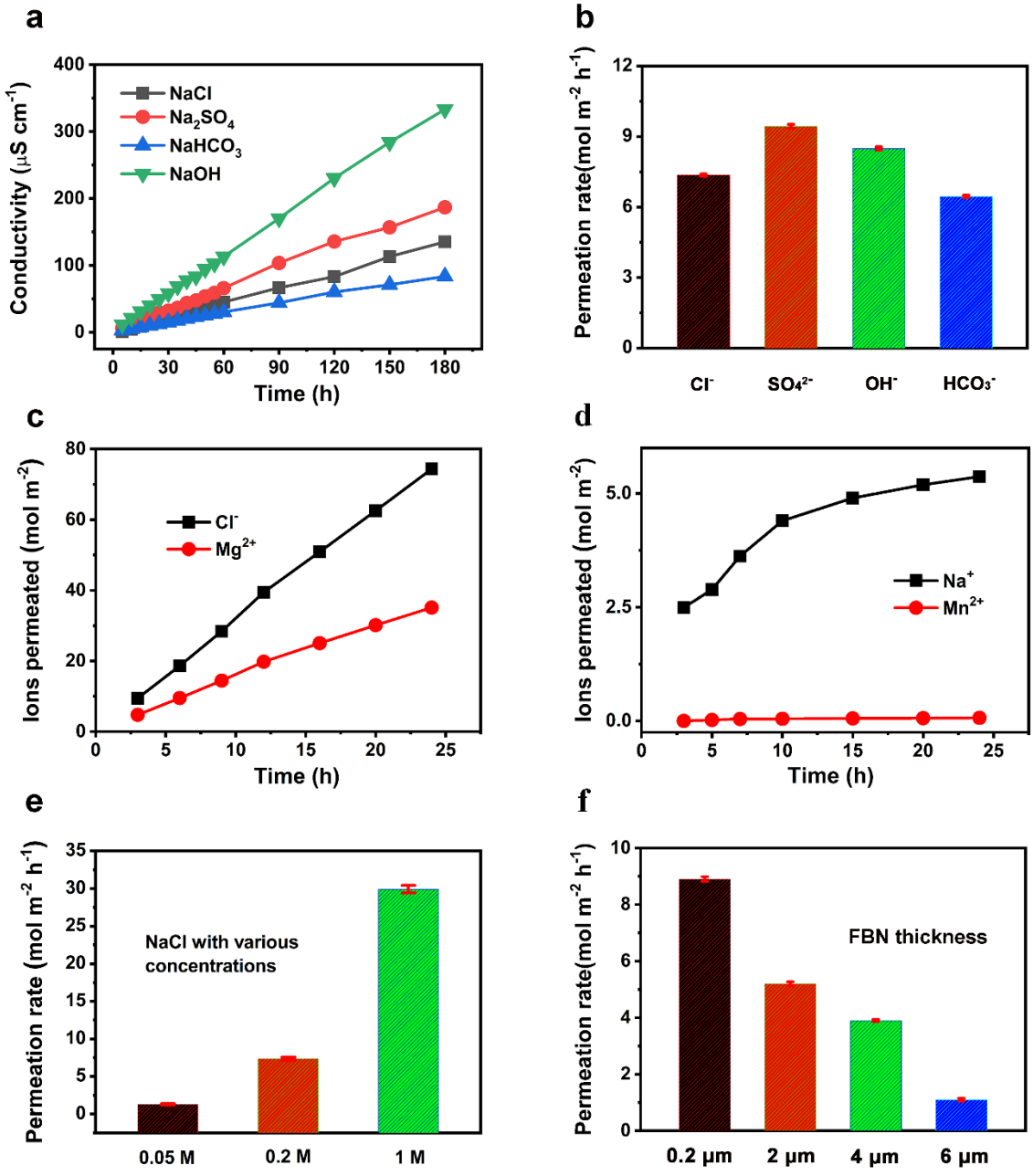

Figure 2. Permeation behaviour of various salts. (a) Ionic conductivity in the permeate compartment versus time of various studied Na salts through FBN membrane, the concentrate of the Na^+ ions were 0.2 M in the feed. (b) Permeation of sodium ions through the FBN membrane

with sodium salts with different anions, concentrations of Na^+ ions were 0.2 M in the feed. (c) Permeation of hydrated Mg^{2+} and Cl^- ions versus time respectively through a FBN membrane with a 0.2 M $MgCl_2$ as the feed. (d) The permeation of hydrated Na^+ and hydrated Mn^{2+} from a feed solution containing 0.2 M NaCl and 0.2 M $MnSO_4$. The permeation rates of Na^+ versus the feed concentration (e), and versus the thickness of FBN on the membrane (f).

A series of ion and molecular-penetration experiments were performed with two homemade plastic compartments separated by an FBN membrane, as shown in the schematic diagram of Figure 1e. The membranes were glued leaving an effective area of 8×10^{-2} cm^2 exposed to the solution. Deionized water (100 mL) was added in both compartments of the device 4 hours in advance to fully hydrate the FBN membrane. Various salt solutions containing alkali, alkaline earth cations or organic molecules were filled in the feed compartment of the device, the other side was filled with equivalent volume of deionized water. The electrical conductivity was recorded at a fixed permeation time on the permeated side to monitor whether any of the solutes permeated into the deionized water through the FBN membrane. The conductivity value reflects the ionic concentration in the permeate compartment.

For small hydrated radii cations (e.g. sodium ion), the conductivity in the permeate compartment exhibited similar increasing tendencies versus time with various salt solutions (Figure 2a, Figure S7). This suggests that the total permeated cations through the FBN membrane follows a time dependant relationship. To quantify the permeation rates of ions, atomic adsorption spectroscopy was used to measure the concentration of and all data were normalized. As shown in Figure 2b, the permeation rate of sodium ion was affected by the corresponding anions, exhibiting different permeation rates in the approximate order of Na_2SO_4>NaOH> NaCl >$NaHCO_3$. For Na_2SO_4 (divalent anion–cation pairs), the higher ionic strength induces a higher osmotic pressure

in the feed solution and a smaller Debye length which results in a faster permeation sodium ions than the other salts (monovalent cation–anion pairs)[29]. The hydrated sodium ion with SO_4^{2-} as counterpart showed a higher permeation rate of 9.2 mol m^{-2} h^{-1} than other types of anions. Then, the alkaline medium makes the BN nanoflakes surface highly ionic and chemically active. The FBN membrane show a slightly better permeation with OH^- than with in neutral conditions. In weak basic condition (e.g. $NaHCO_3$), sodium ion has a slightly reduced permeation (6.3 mol m^{-2} h^{-1}.) than the neutral conditions (e.g. NaCl, 7.3 mol m^{-2} h^{-1}.) possibly due to the hydrolysis and lower mobility of HCO_3^- and side reactions with the function groups on the FBN similar to that observed on graphene oxide surface[30].

Additionally, inductively coupled plasma optical emission spectrometry was employed to quantify the anions. Taking $MgCl_2$ as an example (Figure 2c), the concentrations of hydrated $Mg^{2+}$and Cl^- in the permeate compartment increased linearly with time. The corresponding slops reflected the permeation rates. Hydrated $Mg^{2+}$and Cl^- move through FBN membranes in stable stoichiometric amounts as time increasing. Thus, the permeation of one hydrated Mg^{2+} ion is accompanied by two Cl^- ions, leading to an electric neutral state of the solutions.

In a mixed solution containing both small hydrated cations Na^+ and larger hydrated cations Mn^{2+} (0.2 M NaCl and 0.2 M $MnSO_4$) (Figure 2d), hydrated Na^+ can permeate thought the FBN membrane with concentration increased with testing time, while hydrated Mn^{2+} did not permeate through in the same time. However, the permeation rate of sodium ion in the mixed solution was slower than that in the solution containing only NaCl, possibly due to the larger hydrated Mn^{2+} ions blocking permeation channels of the FBN membrane.

In order to fully understand the rates of ions passing through the FBN membrane, a series parallel tests were conducted. Besides the intrinsic nature of ions (mass, size, charge, etc), the

permeation rate also was affected by the feed concentration. The permeation rates of sodium ions increased linearly with the concentration of the feed solutions (Figure 2e), while the loading of the FBN itself affected the rates inversely (Figure 2f). These results suggest that the permeation rates through FBN membrane could be feasibly tuned to suit the need for different applications. The surface morphology of FBN membranes were observed by SEM before and after ion permeation test. SEM images (Figure S8) show that the continuous structure of the FBN membranes has no obvious change after ion permeation test.

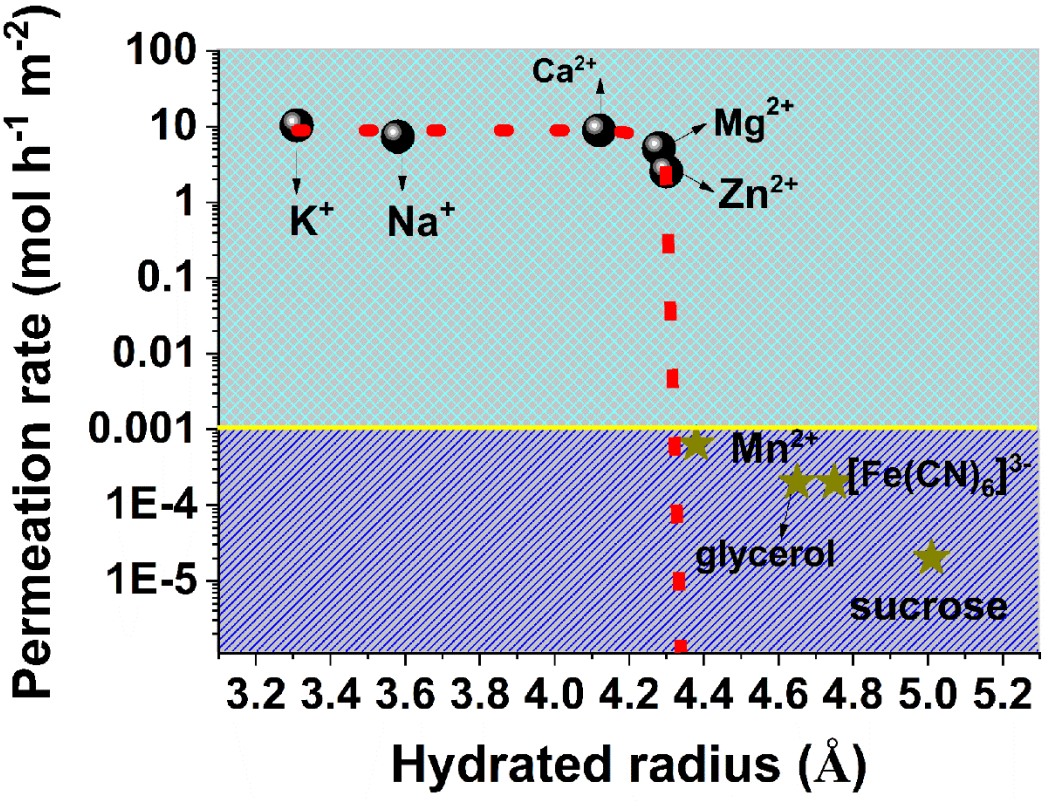

Figure 3. Permeation rates of various hydrated ions and molecules through FBN membrane. Ions shown above the yellow line can pass through the FBN membrane with high permeation rates while ions and molecules below have permeation rates lower than 1×10^{-3} mol h^{-1} m^{-2}.

We tested permeation rate through the FBN membrane with a range of ions and molecules of different sizes (Figure 1e and 1f). The permeation tests were carried out under the same conditions (0.2 M, 298 K, 0.2 μm, 3h) and plotted versus hydrated radii of all species[31, 32]. The results show that the ions permeation rates are dependent on the hydrated radii of the ions. Small ions and molecules can pass through the nanochannels in the FBN membrane with similar permeation rates, while larger molecules are blocked. As shown in Figure 3, there was an abrupt cut-off at ~4.3 Å. It means that hydrated ions species radii larger than this value are sieved out. Therefore, the FBN membrane served as a mesh with a pore size of ~ 8.6 Å physically.

Further insights into the permeation mechanism come from experiments using small angle X-ray scattering (SAXS)[23]. The stacking of FBN nanosheets leaves an intersheet d spacing from 22.4 up to 26 Å according to the Bragg's law ($d=2\pi/q$), which reflects the conceptional distance from the centre of one sheet to another in the stacking direction. In view of the electronic clouds around boron nitride sheets occupying a range of a=3.5 Å[33], and average layer number n of the FBN nanosheets is around 5. The aforementioned ordered capillary $\delta = (d - n \times a) = 4.9$ to 8.5 Å, which is in consistent with the observation from the permeation tests with a cut-off hydrated radius at ~ 4.3 Å. These intralayer spacing supply suitable channels for ions and molecules to diffuse.

Furthermore, we compare the theoretical contribution of diffusion through the capillary channel to the high permeation rate. Based on the AFM and SEM results, the FBN membrane contains FBN flakes with a lateral size distribution averaged at ~200 nm. Therefore, the effective length of the channel can be estimated by $(H / d) \times L$, yielding 20 μm for the FBN membrane with 200 nm thickness. The ions permeation rate, J, contributed from the diffusion through the capillary network can be calculated by the classical diffusion equation[34, 35]:

$$J = D \times \Delta C \times A_{eff} / L_{eff}, \quad (1)$$

where D is the diffusion coefficient (10^{-5} cm^2 s^{-1}) for small ions in water, ΔC is the concentration gradient (≈ 0.2×23 g L^{-1}), and A_{eff} and L_{eff} are the effective area and length of the water column, respectively (Please refer to Experimental section for details about ion permeation rates calculation). Therefore, the measured permeation rate of the FBN nanocapillary network (9 mol h^{-1} m^{-2}) is around 25 times larger than theoretical diffusion rate (0.36 mol h^{-1} m^{-2}). These results are larger than the results of GO membrane (measured rate: around 1 mol h^{-1} m^{-2} and theatrical rate: around 5×10^{-4} mol h^{-1} m^{-2})[31] due to the smaller FBN flakes and thinner FBN membrane. Three aspects accounts for such results. First, the FBN lamellar membrane keeps negative charged (−33 mV) even been densely restacked[36]. Then, the nanosized BN flakes with 1.2 nm in thickness and 100-300 nm in size account for the variety of nanochannel for the hydrated ions passing through the FBN membrane, which is similar to other 2D membranes[37, 38]. Third, the thin FBN membrane (200 nm) showed an effective length of L_{eff} (≈ 20 μm), which significantly decreased the length of ions transport routes compared to GO membrane (5 μm in thickness and L_{eff} of 0.5 cm)[31].

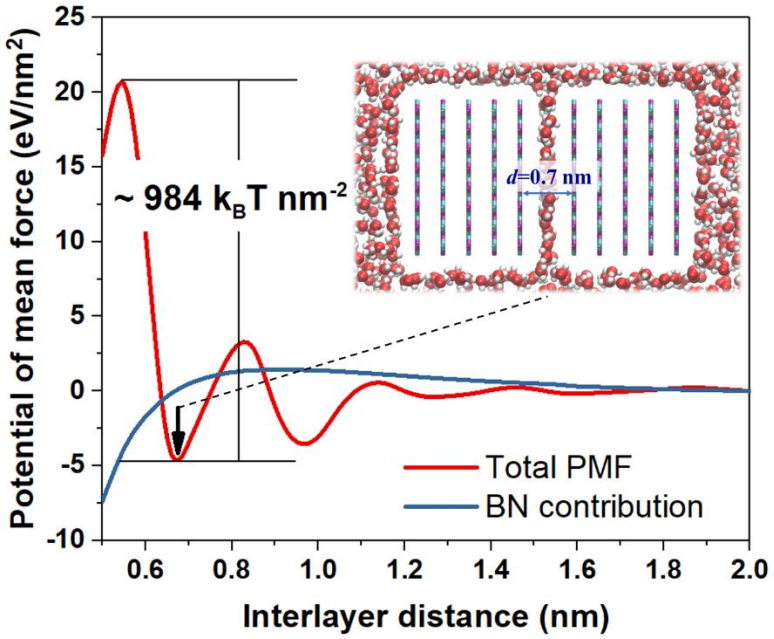

Figure 4. Potential of mean force (PMF) of BN flakes solvated in water (red), and direct BN/BN interaction potential (blue) versus interlayer separation, *d*, between two parallel BN sheets, (each contains five AA' stacked BN layers). Inset shows the schematic of BN flakes in water at *d*=0.7 nm, where monolayer water is found between flakes. The desorption energy of the monolayer water is ~984 $k_{\mathrm{B}}T$ nm^{-2}.

To further understand the above observation, we used molecular dynamics (MD) simulations to investigate the stability of the BN flakes in water. The potential of mean force (PMF) was calculated by numerically integrating the interaction forces required to separate the two parallel and fixed BN flakes at various intralayer separations[39]. The reaction coordinates chosen here were demonstrated in a recent work[40]. The interaction force in each window is provided in Figure S4. As shown in Figure 4, we find layered water structures confined between BN sheets could generate an energy barrier, overcoming the van der Waals adhesion between the solids. The figure shows three obvious metastable states of the BN solution at $d \approx 7.0$, 9.5, and 13.0 Å, respectively. For d = 7.0 Å, a monolayer water occupies between the BN flakes. The energy barrier preventing the BN flakes from undergoing aggregation is estimated to be as large as ~984 $k_{\mathrm{B}}T$ nm^{-2}. For an FBN membrane with an area of 8×10^{-4} cm^2 in experiments, the energy barrier is about 13 orders of magnitude larger than $k_{\mathrm{B}}T$. Note that the functional groups on the BN sheets could enlarge the interlayer distance. Here in this calculation the flexibility of the BN layers is also not included, which would further influence the size of the capillary channel. The calculations can provide a molecular understanding that FBN membrane could support suitable nanochannel to allow small molecules to pass through, making it an excellent molecular sieving membrane.

4. CONCLUSIONS

In conclusion, the hydrate FBN membranes, down to 8.6 angstroms between exfoliated boron nitride layers (channel size), were developed by a facile filtration method. Small ions (< 8.6 Å), such as Na^+, K^+, Ca^{2+}, Mg^{2+} and Zn^{2+} permeated quickly through the FBN membranes, whereas larger ions and molecules (> 8.6 Å), including Mn^{2+}, $[Fe(CN)_6]^{3-}$, sucrose and glycerol infiltrated much more slowly. Moreover, the FBN membrane showed ultrafast and stable ion and molecular sieving performance in harsh medium. The experimental results and MD simulations provide that the precise nanochannels of FBN membrane account for the ions and molecular sieving applications.

ASSOCIATE CONTENT

Figure S1 shows the AFM image of FBN nanosheets, Figure S2 shows the XRD of the FBN membrane. Figure S3-S6 show the physical and chemical characteristics of the FBN membranes. Figure S7 shows the ionic conductivity in the permeate compartment versus time of various studied ionic compounds through FBN membrane. Figure S8 shows the FBN membrane before and after used for Na^+ - Mn^{2+} sieving. Figure S9 shows the raw PMF data. Table S1 shows the list of analyzed species and their hydrated radii

AUTHOR INFORMATION

Corresponding authors

E-mail: dan.liu@deakin.edu.au;

E-mail: maming16@mail.tsinghua.edu.cn;

E-mail: zhe.liu@unimelb.edu.au;

E-mail: weiwei.lei@deakin.edu.au.

Author Contributions

All authors have contributed to the writing of this work and have given approval to the submission of this manuscript. C.C. and S.Q. contribute equally to this work.

Notes

The authors declare no competing financial interest.

ACKNOWLEDGMENT

The Australian Research Council Discovery Program (DP190103290, DP180102890) and Australian Research Council Discovery Early Career Researcher Award scheme (DE150101617) financially supported this work.

REFERENCES

1. Jirage, K. B.; Hulteen, J. C.; Martin, C. R., Nanotubule-based Molecular-filtration Membranes. *Science* **1997**, 278 (5338), 655-658.

2. McKeown, N. B.; Budd, P. M., Polymers of Intrinsic microporosity (PIMs): Organic Materials for Membrane Separations, Heterogeneous Catalysis and Hydrogen Storage. *Chem. Soc. Rev.* **2006**, 35 (8), 675-683.

3. Gin, D. L.; Noble, R. D., Designing the Next Generation of Chemical Separation Membranes. *Science* **2011**, 332 (6030), 674-676.

4. Cohen-Tanugi, D.; Grossman, J. C., Water Desalination across Nanoporous Graphene. *Nano Lett.* **2012**, 12 (7), 3602-3608.

5. Koenig, S. P.; Wang, L.; Pellegrino, J.; Bunch, J. S., Selective Molecular Sieving through Porous Graphene. *Nat. Nanotechnol.* **2012**, 7 (11), 728-732.

6. Ulbricht, M., Advanced Functional Polymer Membranes. *Polymer* **2006**, 47 (7), 2217-2262.

7. Elimelech, M.; Phillip, W. A., The Future of Seawater Desalination: Energy, Technology, and the Environment. *Science* **2011**, 333 (6043), 712-717.

8. Mi, B., Graphene Oxide Membranes for Ionic and Molecular Sieving. *Science* **2014**, 343 (6172), 740-742.

9. Cote, L. J.; Kim, J.; Zhang, Z.; Sun, C.; Huang, J., Tunable Assembly of Graphene Oxide Surfactant Sheets: Wrinkles, Overlaps and Impacts on Thin Film Properties. *Soft Matter* **2010**, 6 (24), 6096-6101.

10. Stankovich, S.; Dikin, D. A.; Compton, O. C.; Dommett, G. H. B.; Ruoff, R. S.; Nguyen, S. T., Systematic Post-assembly Modification of Graphene Oxide Paper with Primary Alkylamines. *Chem. Mater.* **2010**, 22 (14), 4153-4157.

11. Yeh, C.-N.; Raidongia, K.; Shao, J.; Yang, Q.-H.; Huang, J., On the Origin of the Stability of Graphene Oxide Membranes in Water. *Nat. Chem.* **2015**, 7 (2), 166-170.

12. Zeng, H.; Zhi, C.; Zhang, Z.; Wei, X.; Wang, X.; Guo, W.; Bando, Y.; Golberg, D., "White graphenes": Boron Nitride Nanoribbons via Boron Nitride Nanotube Unwrapping. *Nano Lett.* **2010**, 10 (12), 5049-5055.

13. Chen, Z.-G.; Zou, J.; Liu, G.; Li, F.; Wang, Y.; Wang, L.; Yuan, X.-L.; Sekiguchi, T.; Cheng, H.-M.; Lu, G. Q., Novel Boron Nitride Hollow Nanoribbons. *ACS Nano* **2008**, 2 (10), 2183-2191.

14. Song, L.; Ci, L.; Lu, H.; Sorokin, P. B.; Jin, C.; Ni, J.; Kvashnin, A. G.; Kvashnin, D. G.; Lou, J.; Yakobson, B. I., Large Scale Growth and Characterization of Atomic Hexagonal Boron Nitride Layers. *Nano Lett.* **2010**, 10 (8), 3209-3215.

15. Zhi, C.; Bando, Y.; Tang, C.; Kuwahara, H.; Golberg, D., Large‐scale Fabrication of Boron Nitride Nanosheets and Their Utilization in Polymeric Composites with Improved Thermal and Mechanical Properties. *Adv. Mater.* **2009**, 21 (28), 2889-2893.

16. Gao, R.; Yin, L.; Wang, C.; Qi, Y.; Lun, N.; Zhang, L.; Liu, Y.-X.; Kang, L.; Wang, X., High-yield Synthesis of Boron Nitride Nanosheets with Strong Ultraviolet Cathodoluminescence Emission. *J. Phys. Chem. C* **2009**, 113 (34), 15160-15165.

17. Meng, X. L.; Lun, N.; Qi, Y. Q.; Bi, J. Q.; Qi, Y. X.; Zhu, H. L.; Han, F. D.; Bai, Y. J.; Yin, L. W.; Fan, R. H., Low‐Temperature Synthesis of Meshy Boron Nitride with a Large Surface Area. *ChemistryEur. J. Inorg. Chem.* **2010**, 2010 (20), 3174-3178.

18. Lei, W.; Portehault, D.; Liu, D.; Qin, S.; Chen, Y., Porous Boron Nitride Nanosheets for Effective Water Cleaning. *Nat. Commun.* **2013**, 4, 1777.

19. Lei, W.; Zhang, H.; Wu, Y.; Zhang, B.; Liu, D.; Qin, S.; Liu, Z.; Liu, L.; Ma, Y.; Chen, Y., Oxygen-doped Boron Nitride Nanosheets with Excellent Performance in Hydrogen Storage. *Nano Energy* **2014**, 6, 219-224.

20. Qin, S.; Liu, D.; Wang, G.; Portehault, D.; Garvey, C. J.; Gogotsi, Y.; Lei, W.; Chen, Y., High and Stable Ionic Conductivity in 2D Nanofluidic Ion Channels between Boron Nitride Layers. *J. Am. Chem. Soc.* **2017**, 139 (18), 6314-6320.

21. Pacile, D.; Meyer, J. C.; Girit, Ç.; Zettl, A., The Two-dimensional Phase of Boron Nitride: Few-atomic-layer Sheets and Suspended Membranes. *Appl. Phys. Lett.* **2008**, 92 (13), 133107.

22. Meyer, J. C.; Chuvilin, A.; Algara-Siller, G.; Biskupek, J.; Kaiser, U., Selective Sputtering and Atomic Resolution Imaging of Atomically Thin Boron Nitride Membranes. *Nano Lett.* **2009**, 9 (7), 2683-2689.

23. Chen, C.; Wang, J.; Liu, D.; Yang, C.; Liu, Y.; Ruoff, R. S.; Lei, W., Functionalized Boron Nitride Membranes with Ultrafast Solvent Transport Performance for Molecular Separation. *Nat. Commun.* **2018**, 9 (1), 1902.

24. Chen, C.; Liu, D.; Wang, J.; Wang, L.; Sun, J.; Lei, W., Functionalized Boron Nitride Membranes with Multipurpose and Super-stable Semi-permeability in Solvents. *J. Mater. Chem. A* **2018**, 6 (42), 21104-21109.

25. Plimpton, S., Fast Parallel Algorithms for Short-range Molecular Dynamics. *J. Comput. Phys.* **1995**, 117 (1), 1-19.

26. Tocci, G.; Joly, L.; Michaelides, A., Friction of Water on Graphene and Hexagonal Boron Nitride from Ab Initio Methods: Very Different Slippage Despite Very Similar Interface Structures. *Nano Lett.* **2014**, 14 (12), 6872-6877.

27. Ryckaert, J.-P.; Ciccotti, G.; Berendsen, H. J. C., Numerical Integration of the Cartesian Equations of Motion of a System with Constraints: Molecular Dynamics of N-alkanes. *J. Comput. Phys.* **1977**, 23 (3), 327-341.

28. Lei, W.; Mochalin, V. N.; Liu, D.; Qin, S.; Gogotsi, Y.; Chen, Y., Boron Nitride Colloidal Solutions, Ultralight Aerogels and Freestanding Membranes through One-step Exfoliation and Functionalization. *Nat. Commun.* **2015**, 6, 8849.

29. Cheng, C.; Jiang, G.; Simon, G. P.; Liu, J. Z.; Li, D., Low-voltage Electrostatic Modulation of Ion Diffusion Through Layered Graphene-based Nanoporous Membranes. *Nat. Nanotechnol.* **2018**, 13, 685-690.

30. Sun, P.; Zhu, M.; Wang, K.; Zhong, M.; Wei, J.; Wu, D.; Xu, Z.; Zhu, H., Selective Ion Penetration of Graphene Oxide Membranes. *ACS Nano* **2012**, 7 (1), 428-437.

31. Joshi, R. K.; Carbone, P.; Wang, F. C.; Kravets, V. G.; Su, Y.; Grigorieva, I. V.; Wu, H. A.; Geim, A. K.; Nair, R. R., Precise and Ultrafast Molecular Sieving through Graphene Oxide Membranes. *Science* **2014**, 343 (6172), 752-754.

32. Nightingale Jr, E. R., Phenomenological Theory of Ion Solvation. Effective Radii of Hydrated Ions. *J. Phys. Chem.* **1959**, 63 (9), 1381-1387.

33. Lin, Y.; Williams, T. V.; Xu, T.-B.; Cao, W.; Elsayed-Ali, H. E.; Connell, J. W., Aqueous Dispersions of Few-layered and Monolayered Hexagonal Boron Nitride Nanosheets from Sonication-assisted Hydrolysis: Critical Role of Water. *J. Phys. Chem. C* **2011**, 115 (6), 2679-2685.

34. Jiang, G.; Wang, P.; Cheng, C.; Li, D.; Liu, J. Z., An equivalent 1D Nanochannel Model to Describe Ion Transport in Multilayered Graphene Membranes. *Prog. Nat. Sci.* **2018**, 28 (2), 246-250.

35. Cheng, C.; Jiang, G.; Garvey, C. J.; Wang, Y.; Simon, G. P.; Liu, J. Z.; Li, D., Ion Transport in Complex Layered Graphene-based Membranes with Tuneable Interlayer Spacing. *Sci. Adv.* **2016**, 2 (2), e1501272.

36. Koltonow, A. R.; Huang, J., Two-dimensional Nanofluidics. *Science* **2016**, 351 (6280), 1395-1396.

37. Huang, H.; Song, Z.; Wei, N.; Shi, L.; Mao, Y.; Ying, Y.; Sun, L.; Xu, Z.; Peng, X., Ultrafast Viscous Water Flow through Nanostrand-channelled Graphene Oxide Membranes. *Nat. Commun.* **2013**, 4, 2979.

38. Sun, L.; Ying, Y.; Huang, H.; Song, Z.; Mao, Y.; Xu, Z.; Peng, X., Ultrafast Molecule Separation through Layered WS_2 Nanosheet Membranes. *ACS Nano* **2014**, 8 (6), 6304-6311.

39. Shih, C.-J.; Lin, S.; Strano, M. S.; Blankschtein, D., Understanding the Stabilization of Liquid-phase-exfoliated Graphene in Polar solvents: Molecular Dynamics Simulations and Kinetic Theory of Colloid Aggregation. *J. Am. Chem. Soc.* **2010**, 132 (41), 14638-14648.

40. Cao, W.; Wang, J.; Ma, M., Exfoliation of Two-Dimensional Materials: The Role of Entropy. *J. Phys. Chem. L* **2019**, 981-986.

TOC

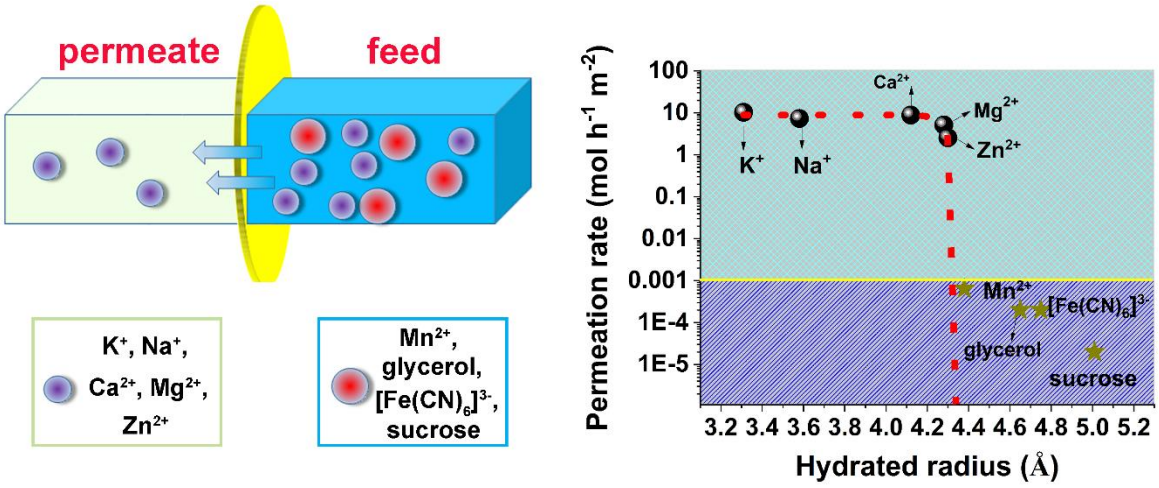
permeate
feed
K+, Na+, Ca2+, Mg2+, Zn2+
Mn2+, glycerol, [Fe(CN)6]3-, sucrose
Permeation rate (mol h-1 m-2)
100
10
1
0.1
0.01
0.001
1E-4
1E-5
K+
Na+
Ca2+
Mg2+
Zn2+
Mn2+
[Fe(CN)6]3-
glycerol
sucrose
3.2 3.4 3.6 3.8 4.0 4.2 4.4 4.6 4.8 5.0 5.2
Hydrated radius (Å)